




Geometric spin Hall effect of a laser beam beyond the paraxial approximation

Mengdi Luo  and Zhaoying Wang *

Zhejiang Province Key Laboratory of Quantum Technology and Device, School of Physics, Zhejiang University, Hangzhou 310027, China

 (Received 19 April 2022; accepted 19 September 2022; published 18 October 2022)

An intriguing spin-orbital angular momentum interaction, called the geometric spin Hall effect of light (GSHEL), has aroused much interest and manifests itself as a transverse shift. The GSHEL of the classical optical field is independent of the beam size. In this paper the GSHELs of the vortex vector continuous wave (VVCW) and vortex ultrashort pulsed beam (VUPB) are systematically analyzed beyond the paraxial approximation. The analytical expression of the transverse shift of the VVCW is obtained. Evidently, the magnitude of the transverse shift depends on the ratio of the beam waist to the wavelength. The transverse shift can be effectively enlarged by narrowing the beam waist even to the order of more than $10\ \mu\text{m}$. This intriguing phenomenon is caused by the stronger spin-orbital interaction induced energy flow in the nonparaxial regime. Furthermore, the GSHEL of the VUPB is also explored. The pulse duration time strongly affects the distribution of the phase. The singularities play a crucial role in altering the orientation of the electric field. As a result, the VUPBs with different pulse duration time have different magnitudes of the GSHEL. These results may find significant applications in the investigation of the particle manipulation, microscopic imaging, and ultrashort optics.

DOI: [10.1103/PhysRevA.106.043512](https://doi.org/10.1103/PhysRevA.106.043512)

I. INTRODUCTION

The angular momentum of light, known as spin angular momentum (SAM) and orbital angular momentum (OAM), plays a crucial role in many fundamental and applied fields [1]. Typically, the spin angular momentum is associated with the polarization, the intrinsic orbital angular momentum is related to the spiral phase, and the extrinsic orbital angular momentum is related to the beam propagation trajectory. However, an interesting phenomenon called the spin Hall effect of light [2–7] appears at the reflection or transmission of light beams at various interfaces and it produces a shift of the left- and right-circularly polarized beams in opposite directions, orthogonal to the plane of propagation. The underlying physical origin of the spin Hall effect is the spin-orbital interaction. The spin Hall transverse shift is usually very tiny at the subwavelength scale. Hosten and Kwiat observed the spin Hall effect while photons passing through an air-glass interface by using the quantum weak measurement [8]. Kim *et al.* demonstrated a gigantic spin Hall effect of light incident polarization at an interface between isotropic and anisotropic media [9].

Aiello *et al.* proposed the concept of the geometric spin Hall effect of light (GSHEL). This is a spin-dependent transverse shift of the barycenter of the energy flux density (Poynting vector) through an oblique cross section of a paraxial optical beam in free space [10]. The SAM and OAM interact in the detector surface of the tilted beam and then generate the transverse components of the angular momentum of the beam in the tilted section. Unlike the conventional spin Hall effect, which depends upon the light-matter interaction,

the GSHEL phenomenon could be observed in an oblique plane with respect to the propagation direction even when a light propagates in free space [11–13]. The underlying physics of the GSHEL can also be interpreted in terms of an effective geometric phase [13]. Much theoretical and experimental research has been carried out on the GSHEL [14–18]. Kong *et al.* explored theoretically the effects of intrinsic orbital angular momentum on the GSHEL and demonstrated that the GSHEL was actually an effect of the total angular momentum and not only SAM [14]. Wang and Chen discussed the GSHEL with respect to momentum flux instead of energy flux [18]. Chen *et al.* investigated a new type of spin-orbital coupling between the longitudinal SAM and transversal OAM carried by a spatiotemporal optical vortex wave packet under a tight focusing condition [19]. Furthermore, an experimental nanoprobeing technique in combination with a reconstruction algorithm has been utilized to demonstrate the GSHEL in a highly nonparaxial beam [15]. In the latest research, an optical spatial differentiator was proposed for achieving edge detection based on a tilted polarized interface to develop new applications for the GSHEL [20]. Compared with traditional computer processing image information, the optical operation has the advantage of high-speed and low-power consumption.

The results from Refs. [14,21] show the transverse shift of the GSHEL with respect to the energy flux as

$$\langle y' \rangle = (\sigma + 2n) \frac{\tan \theta}{2k},$$

where σ denotes the polarization of the beam and n is the topological charge. The transverse shift is related to the wave number k and the tilted angle θ for the vortex vector continuous wave (VVCW). In the experimental research, a strongly focused beam is often chosen to strengthen the phenomenon

*zhaoyingwang@zju.edu.cn

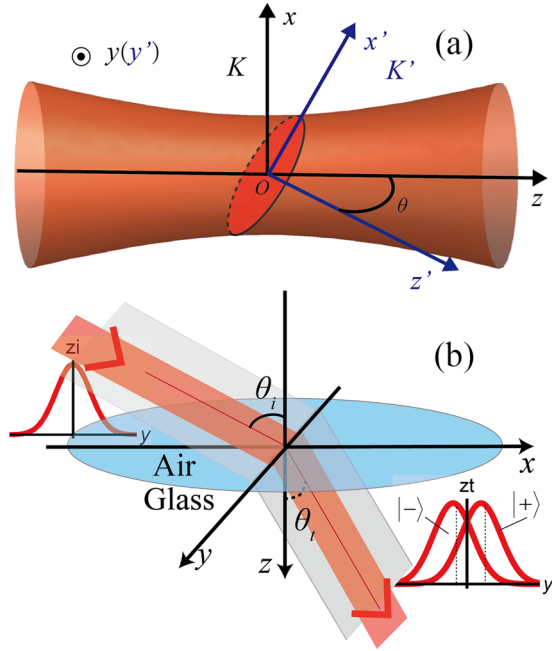


FIG. 1. (a) Geometry of the coordinate system. Here (x, z) and (x', z') represent the beam and the laboratory coordinate systems K and K' , respectively. The coordinate system K rotates in the x - z plane. Note that the beam cross section on the observation plane $z' = 0$ is stretched in the x' direction while the GSHEL occurs in the y' direction. (b) Conventional spin Hall effect at an air-glass interface from Ref. [8].

of the GSHEL for observation. However, here we report on detailed nonparaxial theoretical research.

Additionally, compared with the continuous wave, the ultrashort pulsed beam has an extremely broad frequency spectrum and a strongly space-time coupling effect, resulting in the dependence of intensity and phase distributions on not only the beam waist but also the pulse duration. Therefore, in this paper, the relationship between the transverse shift and pulse duration time is presented as well.

The structure of this paper is as follows. We first briefly introduce the theory of the GSHEL in the tilted coordinate system. Then, based on the vector potential, the analytical expression of the transverse shift of the VVCW is deduced. The dependence of the transverse shift on the ratio of the beam waist to the wavelength is explored, which is caused by the spin-orbital interaction-induced energy flow in the nonparaxial regime. Finally, analogous to the VVCW, the numerical results of the transverse shift of the vortex ultrashort pulsed beam (VUPB) are obtained. Because of the spatiotemporal coupling effect, the pulse duration time strongly influences the phase distributions and the appearance of the singularities of the electromagnetic field, which is crucial in altering the magnitude of the GSHEL. Thus, the pulse duration time can affect the magnitude of the transverse shift.

II. THEORY OF THE GSHEL

Above all, the GSHEL and the underlying physical origin are illustrated in this section. Figure 1 shows the geometry of the generation of the GSHEL and the conventional spin

Hall effect at an air-glass interface from Ref. [8]. As shown in Fig. 1(b), Hosten and Kwist have detected the conventional photonic spin Hall effect for a light passing through an air-glass interface and demonstrated that the spin-dependent displacement is perpendicular to the refractive index gradient. When a photonic wave packet changes the propagation direction because of a spatial variation in the refractive index, the wave components with different wave vectors experience different geometric phases, affecting the spatial profile and resulting in the spin Hall effect of light. Whereas, different from the conventional spin Hall effect of light, the geometrical spin Hall effect of light does not originate in a medium as a result of light-matter interaction, it occurs in vacuum and is determined by the geometry of the beam-detector system only [10], as shown in Fig. 1(a). The coordinate system K rotates in the x - z plane into K' . Thus, the y axis remains unchanged in the coordinate transformation and is presented as y' in the following section. In addition, the GSHEL occurs in the y' direction, which manifests itself as a transverse shift.

Consider a laser beam (continuous wave or pulsed beam) that propagates along the z axis, with the detecting plane tilted by an angle θ against the z axis, as shown in Fig. 1. Thus, in the system K' attached to the reference axis z' , the angular momentum density will have both longitudinal and transversal components. As the cross section of the beam when seen from K' is augmented by a factor $1/\cos\theta$ [14], we find that the longitudinal linear momentum density will go like

$$p'_{z'} = p_z - p_x \tan\theta. \quad (1)$$

The relationship between linear and angular momentum [10] follows that $J'_{x'} = \langle y' \rangle P'_{z'}$ with $z = 0$ and $x = 0$. In Refs. [10,14], the transverse shift of the GSHEL could be expressed as

$$\langle y' \rangle \propto \frac{\int_{-\infty}^{+\infty} y' p'_{z'} dy'}{\int_{-\infty}^{+\infty} p'_{z'} dy'}. \quad (2)$$

We know that when $\theta = 0$, evidently, the transverse shift $\langle y' \rangle$ is zero. If $\theta \neq 0$, $p'_{z'}$ is no longer symmetric about the y axis but has a slight imbalance [22]. This slight imbalance causes the transverse shift in the tilted plane. To physically comprehend the GSHEL phenomenon, we consider that such a shift is the result of a nonzero transverse angular momentum. As a consequence, the transverse shift $\langle y' \rangle$ can be detected in the tilted plane [12,20].

III. THE GSHEL OF THE VORTEX VECTOR CONTINUOUS WAVE

In previous theoretical research on the GSHEL, most of the light fields were analyzed under the paraxial limitation. Actually, the spin-orbital interaction (SOI) effect-induced energy flow phenomenon is more pronounced in the nonparaxial regime. The SOI is the important factor to produce the transverse shift of GSHEL. Therefore, in this paper, all of our calculations about the GSHEL are performed beyond the paraxial approximation. The vector potential and Lorentz gauge are employed in this section to establish the exact solution expression of the VVCW. The vector potential in the

x direction can be written as

$$A_x(\rho) = \frac{\left(\sqrt{\frac{2}{|n|}} \frac{\rho}{w_z}\right)^{|n|}}{\sqrt{z^2/z_R^2 + 1}} \exp[-i(|n| + 1)\Psi(z)] \\ \times \exp\left[\frac{|n|}{2} + \frac{i\rho^2\omega}{2cq_z} - in\phi - i\left(t - \frac{z}{c}\right)\omega\right], \quad (3)$$

where $q_z = z - iz_R$ is the complex beam parameter, $\Psi(z) = \tan^{-1}(z/z_R)$ is the Gouy phase, w_0 is the beam waist, $w_z = w_0\sqrt{1 + z^2/z_R^2}$, and $z_R = kw_0^2/2$ is the Rayleigh distance.

Here we should mention that the direction of the vector potential is set along the x axis. Thus, under the paraxial approximation, the polarization state of a light beam is of linear polarization, whereas for the nonparaxial light beam the spin will appear due to the spin-orbital coupling effect [23–25].

By utilizing the Maxwell equations $\mathbf{E} = -\nabla\varphi - \partial\mathbf{A}/\partial t$ and $\mathbf{B} = \nabla \times \mathbf{A}$, under the condition of the Lorentz gauge $\nabla \cdot \mathbf{A} + \partial\varphi/\partial(c^2t) = 0$ the electric- and magnetic-field components of the VVCW under the condition of $x = 0$ and $z = 0$ can be derived,

$$E_x = iG_{CW}(y)[z_R|n| + k^2y^2z_R - ky^2 - (n^2 + 1)z_R] \exp[-in \tan^{-1}(0, y) - i\omega t], \\ E_y = nG_{CW}(y)(-z_R|n| + ky^2 + z_R) \exp[-in \tan^{-1}(0, y) - i\omega t], \\ E_z = \frac{iny}{2z_R}G_{CW}(y)[2z_R|n| - k(y^2 + 2z_R^2) + 2z_R] \exp[-in \tan^{-1}(0, y) - i\omega t], \\ B_x = 0, \\ B_y = \frac{iky^2}{2cz_R}G_{CW}(y)[k(y^2 + 2z_R^2) - 2z_R|n| - 2z_R] \exp[-in \tan^{-1}(0, y) - i\omega t], \\ B_z = \frac{ky}{c}G_{CW}(y)(ky^2 - z_R|n| + z_R) \exp[-in \tan^{-1}(0, y) - i\omega t], \quad (4)$$

where $\tan^{-1}(x_1, y_1)$ gives the arc tangent of y_1/x_1 , taking into account which quadrant the point (x_1, y_1) is in, and

$$G_{CW}(y) = c|n|^{-|n|/2}z_R^{-|n|/2-1}(ky^2)^{|n|/2-1} \exp\left(\frac{1}{2}|n| - \frac{ky^2}{2z_R}\right).$$

According to the work of Allen *et al.* [21], the time average linear momentum density of the beam can be expressed as

$$\mathbf{p} = \frac{\epsilon_0}{2}(\mathbf{E}^* \times \mathbf{B} + \mathbf{E} \times \mathbf{B}^*). \quad (5)$$

Thus, the three components (p_x , p_y , and p_z) of the linear momentum density in the beam coordinate system K can be obtained from Eq. (5). Due to the symmetry of the linear momentum as shown in Figs. 2(b) and 2(c), by substituting Eq. (1) into Eq. (2), we can obtain the simplified expression of the transverse shift $\langle y' \rangle$:

$$\langle y' \rangle \propto \frac{\int_{-\infty}^{+\infty} y'(p_z - p_x \tan \theta) dy'}{\int_{-\infty}^{+\infty} (p_z - p_x \tan \theta) dy'} = -\frac{\int_{-\infty}^{+\infty} y' p_x \tan(\theta) dy'}{\int_{-\infty}^{+\infty} p_z dy'}. \quad (6)$$

Subsequently, by substituting p_x and p_z into Eq. (6) and after integration of y' with $x = 0$ and $z = 0$, the transverse shift of the intensity barycenter of the VVCW can be obtained as

$$\langle y'_{CW} \rangle = -\frac{n \tan(\theta)[(32|n| - 16)k^2z_R^2 - (32|n|^2 - 16)kz_R + 8|n|^3 + 28|n|^2 + 6|n| - 11]}{4k[(8|n| - 4)k^2z_R^2 - (4|n|^2 + 4|n| + 8n^2 + 1)kz_R + 4n^2|n| - 2|n| + 10n^2 + 7]}, \quad (7)$$

where $kz_R = 2\pi^2(w_0/\lambda)^2$. In Eq. (7), the shifts caused by the spin and the orbital angular momentum are not separated. We consider the transverse shift resulting from the total angular momentum (AM). It is worth noting that the lateral displacement depends not only on the topological charge, but also on the ratio of the beam waist to the wavelength, in addition to the wave number and the inclination angle. While we set $w_0 \rightarrow \infty$, the GSEHL attains a feature of the paraxial VVCW, i.e., $\langle y'_{CW} \rangle = -n \tan(\theta)/k$, which is consistent with the classical results of Ref. [14]. However, if the beam waist w_0 reduces to subwavelength order, the polarization of the VVCW is changed from linear to circular polarization, which introduces the conversion of the orbital AM to the spin AM.

The SOI inducing the energy flow makes the GSHEL different from the paraxial VVCW. According to Ref. [26], the minimum beam waist of the VVCW and VUPB is dependent on pulse duration time and topological charge. Thus, based on the result from [26], we choose $w_0 = 0.5\lambda$ to mimic the nonparaxial condition in Fig. 2. For the paraxial approximation, we choose $w_0 = 1$ mm as an example, which is about 1580λ when $\lambda = 632.8$ nm.

In Fig. 2(a) we explore the transverse shift of the VVCW as a function of tilted angle θ with the indicated values of beam waist and topological charge n . First, the sign of the topological charge changes the direction of the transverse shift. Meanwhile, the value of the transverse shift varies with the

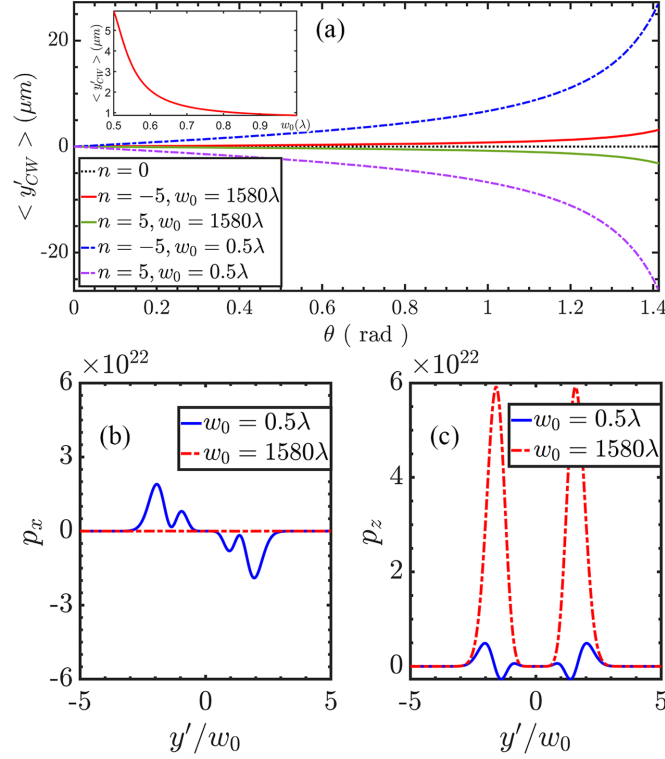


FIG. 2. Transverse shift of the GSHEL for the VVCW in the y' direction as a function of the tilted angle θ for the indicated values of the topological charge and beam waist. The inset shows the relationship between the beam waist and $\langle y'_{CW} \rangle$. Also depicted are the (b) x and (c) z components of linear momentum as a function of y' .

beam waist. As shown in the inset of Fig. 2(a), the transverse shift decreases with the increase of the beam waist and finally tends to $n \tan \theta / k$. This phenomenon is caused by the SOI-induced energy flow in the nonparaxial regime. In this paper, the vector potential we set is in the x direction from Eq. (3). Thus, under the condition of the paraxial approximation, E_x is dominant and the VVCW is of linear polarization. Then the magnitude of p_z is far larger than that of p_x when the beam waist $w_0 = 1580\lambda$, as presented in Figs. 2(b) and 2(c). Nevertheless, beyond the paraxial approximation, the appearance of E_y and E_z causes that p_x and p_z to be almost of the same order. According to Eq. (6), the existence of transverse linear momentum p_x makes the magnitude of transverse shift with $w_0 = 0.5\lambda$ substantially larger than that with $w_0 = 1580\lambda$. The magnitude of the transverse shift can therefore be of more than $10\text{-}\mu\text{m}$ order, which may find significant application in spatial differential operation and edge detection [20].

IV. THE GSHEL OF THE VORTEX ULTRASHORT PULSED BEAM

Controlling the magnitude of the transverse shift is an extremely intriguing and important researching content. In Sec. III we have explored that the much smaller beam waist effectively enlarges the transverse shift of the GSHEL, which

results from the SOI-induced energy flow. In our previous paper [26] we proved that the pulse duration time of the VUPB also influences the distributions of the intensity and phase. Compared with the continuous wave, the VUPB not only couples the time and space but also combines the high-intensity density and OAM, which can be employed in the ultrafast physical process [27–29], materials processing [30–32], and nonlinear optics [33–35]. Thus, in this section, we analyze the transverse shift of the VUPB.

When analyzing the transverse shift of the VUPB, we utilize the same method as for the VVCW to construct the electromagnetic field of the VUPB. The vector potential of the VUPB can be written as [26,36]

$$A_x(\rho, t) = \frac{\exp[-i(|n| + 1)\Psi(z) - in\phi]}{\sqrt{1 + (z/z_R)^2}} \left(\sqrt{\frac{2}{|n|}} \frac{\rho}{w_z} \right)^{|n|} \left[\frac{-i(\alpha + \frac{|n|}{2})}{\omega(t - \frac{z}{c} - \frac{\rho^2}{2cq_z}) - i\alpha} \right]^{\alpha + |n|/2 + 1/2}, \quad (8)$$

where α is the pulse duration time parameter. Therefore, the electromagnetic field of the VUPB under the condition of $x = 0$ and $z = 0$ can be expressed as

$$\begin{aligned}
 E_x &= iG_{\text{pulse}}(y, t)\{2z_R n[-2\omega^2 t^2 z_R + i\omega t(ky^2 + 4\alpha z_R) + \alpha(2k^2 y^2 z_R + ky^2 + 2\alpha z_R)] \\
 &\quad + k^2 y^2 z_R^2 |n|^2 + [4\omega^2 t^2 z_R^2 - n^2(ky^2 + 2i\omega t z_R)^2 - 2ik\omega t y^2 z_R(2\alpha + 1) - 2\alpha k^2 y^4 + k^2 y^2 z_R^2(4\alpha^2 - 1)] \\
 &\quad - 2\alpha z_R[ky^2(2\alpha + 2n^2 + 1) + 4i\omega t z_R(n^2 + 1)] - 4\alpha^2 z_R^2(n^2 + 1)\}, \\
 E_y &= 2nz_R G_{\text{pulse}}(y, t)(2\alpha + |n|)[i\omega t z_R + \alpha(ky^2 + z_R) - |n|(\alpha z_R + i\omega t z_R)], \\
 E_z &= \frac{iny}{2z_R} G_{\text{pulse}}(y, t)(2\alpha z_R + ky^2 + 2i\omega t z_R) \\
 &\quad \times [|n|(4\alpha z_R + 4i\omega t z_R + ky^2 - 2kz_R^2) + 2z_R(2i\omega t - 2\alpha kz_R + kz_R) + ky^2(3 - 2\alpha) + 4\alpha z_R], \\
 B_x &= 0, \\
 B_y &= -\frac{iky^2}{2c} G_{\text{pulse}}(y, t)(2\alpha + |n| - 1) \\
 &\quad \times [|n|(4\alpha z_R + 4i\omega t z_R + ky^2 - 2kz_R^2) - 2z_R(-2i\omega t + 2\alpha kz_R + kz_R) + ky^2(1 - 2\alpha) + 4\alpha z_R], \\
 B_z &= \frac{2z_R ky}{c} G_{\text{pulse}}(y, t)(2\alpha + |n| - 1)[z_R(i\omega t + \alpha)(1 - |n|) + ky^2(\alpha + 1)],
 \end{aligned} \tag{9}$$

where

$$G_{\text{pulse}}(y, t) = \frac{cz_R^{\alpha-1/2} |n|^{-|n|/2} (ky^2)^{|n|/2-1} e^{-in \tan^{-1}(0,y)}}{(2\alpha + |n| - 1)(2\alpha + |n|)} \left(\frac{2\alpha + |n|}{2\alpha z_R + ky^2 + 2i\omega t z_R} \right)^{\alpha+|n|/2+3/2}.$$

Different from the VVCW, the pulse duration time of the VUPB is of the femtosecond timescale, which results in a strong time-space coupling effect. The linear momentum density is time dependent, which is expressed as Eq. (10). Therefore, Eq. (6) is transformed into a two-dimensional integration by integrating the y axis and time [37–39], as shown in Eq. (11). According to Parseval's theorem, the t integrals can be transformed into ω integrals. That is to say, the transverse shift of the VUPB we present in this paper is the average contribution of all frequency components of the beam

$$\mathbf{p} = \frac{\varepsilon_0}{2} \text{Re}[\mathbf{E}] \times \text{Re}[\mathbf{B}], \tag{10}$$

$$\langle y'_{\text{UP}} \rangle = \frac{\int_{-\infty}^{+\infty} \int_{-\infty}^{+\infty} y' p'_z dt dy'}{\int_{-\infty}^{+\infty} \int_{-\infty}^{+\infty} p'_z dt dy'}. \tag{11}$$

To compare with the results of the VVCW, we give the numerical calculating results of the transverse shift of the VUPB in Fig. 3 with the values of the beam waist and the pulse duration time indicated. We can find that the difference of the transverse shift is negligible between the VVCW and VUPB when the beam waist $w_0 = 1580\lambda$. This is because under the condition of the paraxial approximation, E_x is still dominant and the VUPB is also of linear polarization; thus there is still no transverse linear momentum. Nevertheless, when the beam waist reduces to the subwavelength order, e.g., 0.5λ , the shifts for both the VVCW and the VUPB increase due to the appearance of the transverse linear momentum as shown in Figs. 4(a ii) and 4(a iii). However, the amplitude of the transverse shift of the VUPB is smaller than that of the VVCW. The relationship between the transverse shift and the pulse duration time is plotted in the inset of Fig. 3. The magnitude of the transverse shift increases with the increase

of the pulse duration time and finally tends to be constant, consistent with Eq. (7).

Let us focus on the GSHEL for different pulse duration time when the beam waist $w_0 = 0.5\lambda$. Figures 4(a) and 4(b) comparatively show the linear momentum p_z of the VUPB with $\alpha = 5$ and $\alpha = 300$ in the y' - z plane, respectively. When $z = 0$, for the short pulse ($\alpha = 5$), the linear momentum does not have singularity along the y' axis, except the center one. However, in the case of a long pulse ($\alpha = 300$), two singularities exist along the y' axis besides the center one, resulting in the opposite directions of the energy flow on the two sides of one singularity [40–43]. Furthermore, we find that it is the different orientations of the electric field that cause the p_z moving towards different directions, as presented in Figs. 4(a i) and 4(b i). With the increase of the pulse duration time, one can notice that the singularities appear away from

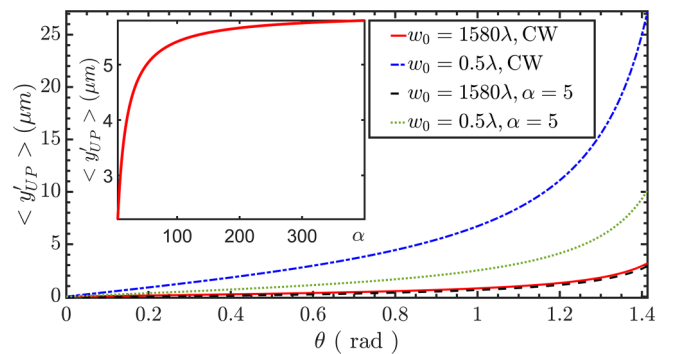


FIG. 3. Transverse shifts of the VUPB and the VVCW in the y' direction as a function of the tilted angle θ with the indicated values of $n = -5$, pulse duration time, and beam waist. The inset shows the relationship between the pulse duration time α and $\langle y'_{\text{UP}} \rangle$.

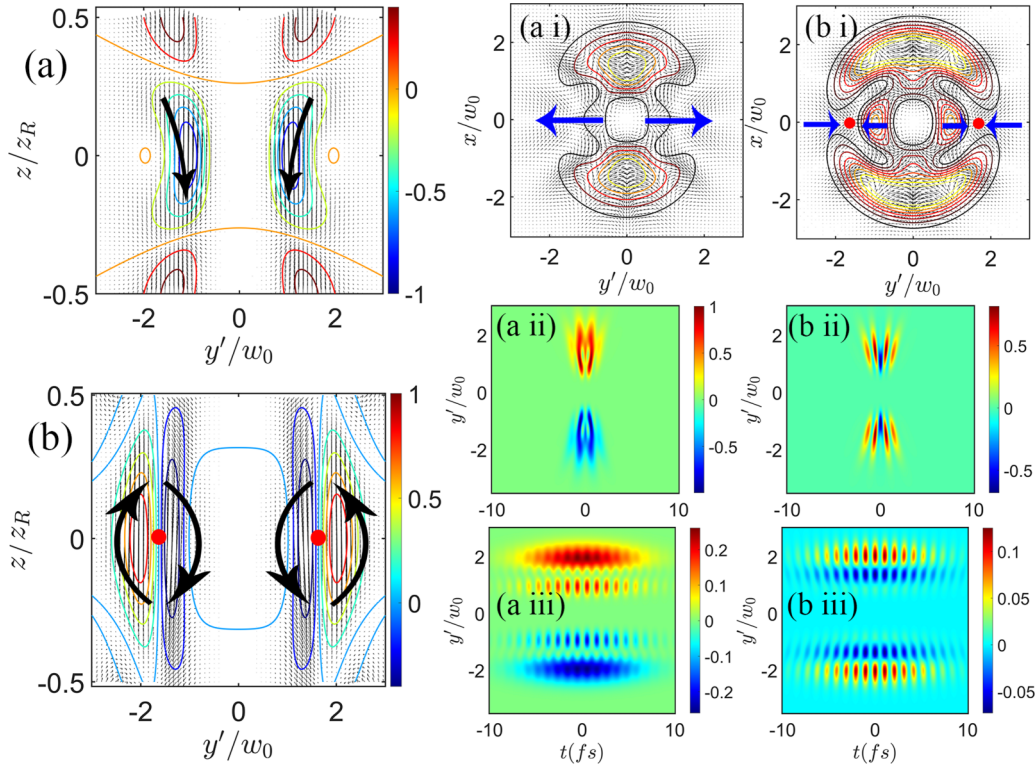


FIG. 4. Arrow plots of the linear momentum and contour plots of the z component of linear momentum in the y' - z plane with (a) $\alpha = 5$ and (b) $\alpha = 300$. Electric-field distributions in the transverse planes are shown for (a i) $\alpha = 5$ and (b i) $\alpha = 300$. The magnitude of the x components is plotted as contours, while the field orientations is presented by arrow plots. The red circles mark the field singularity and the black and blue arrows represent the direction of the field. Also represented are the spatiotemporal distributions of the x and z components of normalized linear momentum with (a ii) and (a iii) $\alpha = 5$ and (b ii) and (b iii) $\alpha = 300$.

the coordinate origin ($x = 0, y' = 0$) [44] along the y' axis. As a result, besides the center one, the short pulse has no singularity and the electric field is oriented outward [Fig. 4(a i)], whereas the long pulse has two singularities along the y' axis and the orientation of the electric field is towards the singularity [Fig. 4(b i)]. That is the main reason why the p_z of the long pulse exhibits an oscillation of positive and negative values along the y' axis, whereas the oscillation vanishes with for the short pulse, as shown in Figs. 4(b ii) and 4(b iii). Thus, the difference in the distribution of the p_z is intuitively attributed to the shift of the singularity caused by the pulse duration time [26]. As a result, the value of p_z with $\alpha = 300$ after integration is smaller than that with $\alpha = 5$. The magnitude of the GSHEL with $\alpha = 5$ is consequently much smaller than that with $\alpha = 300$.

V. CONCLUSION

In summary, in this paper we mainly explored the GSHEL of both the VVCW and VUPB beyond the paraxial approximation, which manifests itself as an OAM- and SAM-dependent transverse shift. By employing the vector

potential, the analytical expression of the transverse shift of the VVCW was obtained and the dependence on the ratio of the beam waist to the wavelength was analyzed. If the wavelength is fixed, the amplitude of the transverse shift is enlarged with a smaller beam waist to more than $10\text{-}\mu\text{m}$ order in this paper, which has advantages in microscopic image. This phenomenon can be attributed to the spin-orbital interaction-induced energy flow among the three components in the nonparaxial regime. When the beam waist is of sub-wavelength, the y and z components of the electric field appear and then the transverse linear momentum becomes larger, which leads to a larger transverse shift.

Furthermore, we also investigated the transverse shift of the VUPB in the case of a smaller waist. Compared with the VVCW, the pulse duration time of the VUPB strongly influences the distributions of the phase distribution as well as the appearance of the singularities, which causes the change of the orientation of the linear momentum. Consequently, the magnitude of the transverse shift varies with the pulse duration time. Thus, the pulse duration time is another way to manipulate the transverse shift, which broadens the potential application of the GSHEL in ultrashort optics.

[1] S. Franke-Arnold, L. Allen, and M. Padgett, Advances in optical angular momentum, *Laser Photon. Rev.* **2**, 299 (2008).

[2] A. Y. Bekshaev, K. Y. Bliokh, and F. Nori, Transverse Spin and Momentum in Two-Wave Interference, *Phys. Rev. X* **5**, 011039 (2015).

- [3] K. Y. Bliokh, D. Smirnova, and F. Nori, Quantum spin Hall effect of light, *Science* **348**, 1448 (2015).
- [4] K. Y. Bliokh and Y. P. Bliokh, Conservation of Angular Momentum, Transverse Shift, and Spin Hall Effect in Reflection and Refraction of an Electromagnetic Wave Packet, *Phys. Rev. Lett.* **96**, 073903 (2006).
- [5] H. Luo, S. Wen, W. Shu, and D. Fan, Spin-to-orbital angular momentum conversion in spin hall effect of light, *Opt. Commun.* **285**, 864 (2012).
- [6] K. Y. Bliokh, F. J. Rodríguez-Fortuño, F. Nori, and A. V. Zayats, Spin-orbit interactions of light, *Nat. Photon.* **9**, 796 (2015).
- [7] K. Y. Bliokh, C. T. Samlan, C. Prajapati, G. Puentes, N. K. Viswanathan, and F. Nori, Spin-Hall effect and circular birefringence of a uniaxial crystal plate, *Optica* **3**, 1039 (2016).
- [8] O. Hosten and P. Kwiat, Observation of the spin Hall effect of light via weak measurements, *Science* **319**, 787 (2008).
- [9] M. Kim, D. Lee, and J. Rho, Incident-polarization-independent spin Hall effect of light reaching half beam waist, *Laser Photon. Rev.* **16**, 2100510 (2022).
- [10] A. Aiello, N. Lindlein, C. Marquardt, and G. Leuchs, Transverse Angular Momentum and Geometric Spin Hall Effect of Light, *Phys. Rev. Lett.* **103**, 100401 (2009).
- [11] A. Y. Bekshaev, Oblique section of a paraxial light beam: Criteria for azimuthal energy flow and orbital angular momentum, *J. Opt. A* **11**, 094003 (2009).
- [12] J. Koger, A. Aiello, V. Chille, P. Banzer, C. Wittmann, N. Lindlein, C. Marquardt, and G. Leuchs, Observation of the Geometric Spin Hall Effect of Light, *Phys. Rev. Lett.* **112**, 113902 (2014).
- [13] X. Ling, X. Zhou, K. Huang, Y. Liu, C. W. Qiu, H. Luo, and S. Wen, Recent advances in the spin Hall effect of light, *Rep. Prog. Phys.* **80**, 066401 (2017).
- [14] L.-J. Kong, S.-X. Qian, Z.-C. Ren, X.-L. Wang, and H.-T. Wang, Effects of orbital angular momentum on the geometric spin Hall effect of light, *Phys. Rev. A* **85**, 035804 (2012).
- [15] M. Neugebauer, P. Banzer, T. Bauer, S. Orlov, N. Lindlein, A. Aiello, and G. Leuchs, Geometric spin Hall effect of light in tightly focused polarization-tailored light beams, *Phys. Rev. A* **89**, 013840 (2014).
- [16] X. Ling, X. Zhou, and X. Yi, Geometric spin Hall effect of light with inhomogeneous polarization, *Opt. Commun.* **383**, 412 (2017).
- [17] K. Y. Bliokh, C. Prajapati, C. T. Samlan, N. K. Viswanathan, and F. Nori, Spin-Hall effect of light at a tilted polarizer, *Opt. Lett.* **44**, 4781 (2019).
- [18] Z.-L. Wang and X.-S. Chen, Anomalous geometric spin Hall effect of light, *Phys. Rev. A* **99**, 063832 (2019).
- [19] J. Chen, L. Yu, C. Wan, and Q. Zhan, Spin-orbit coupling within tightly focused circularly polarized spatiotemporal vortex wavepacket, *ACS Photon.* **9**, 793 (2022).
- [20] S. He, J. Zhou, S. Chen, W. Shu, H. Luo, and S. Wen, Spatial differential operation and edge detection based on the geometric spin hall effect of light, *Opt. Lett.* **45**, 877 (2020).
- [21] L. Allen, M. W. Beijersbergen, R. J. Spreeuw, and J. P. Woerdman, Orbital angular momentum of light and the transformation of Laguerre-Gaussian laser modes, *Phys. Rev. A* **45**, 8185 (1992).
- [22] Z. Zou, R. Lirette, and L. Zhang, Orbital Angular Momentum Reversal and Asymmetry in Acoustic Vortex Beam Reflection, *Phys. Rev. Lett.* **125**, 074301 (2020).
- [23] Y. Shen and C. Rosales-Guzmán, Nonseparable states of light: From quantum to classical, *Laser Photon. Rev.* **16**, 2100533 (2022).
- [24] Y. Shen, Rays, waves, SU(2) symmetry and geometry: toolkits for structured light, *J. Opt.* **23**, 124004 (2021).
- [25] C. Rosales-Guzmán, B. Ndagano, and A. Forbes, A review of complex vector light fields and their applications, *J. Opt.* **20**, 123001 (2018).
- [26] M. Luo and Z. Wang, Angular momentum of the vortex ultrashort pulsed beam with a smaller beam waist, *Opt. Express* **29**, 28597 (2021).
- [27] L. Zhang, B. Shen, Z. Bu, X. Zhang, L. Ji, S. Huang, M. Xiriai, Z. Xu, C. Liu, and Z. Xu, Vortex Harmonic Generation by Circularly Polarized Gaussian Beam Interacting with Tilted Target, *Phys. Rev. Appl.* **16**, 014065 (2021).
- [28] Y.-T. Hu, J. Zhao, H. Zhang, Y. Lu, W.-Q. Wang, L.-X. Hu, F.-Q. Shao, and T.-P. Yu, Attosecond γ -ray vortex generation in near-critical-density plasma driven by twisted laser pulses, *Appl. Phys. Lett.* **118**, 054101 (2021).
- [29] C. Hernández-García, J. S. Román, L. Plaja, and A. Picón, Quantum-path signatures in attosecond helical beams driven by optical vortices, *New J. Phys.* **17**, 093029 (2015).
- [30] J. J. Nivas, H. Shutong, K. K. Anoop, A. Rubano, R. Fittipaldi, A. Vecchione, D. Paparo, L. Marrucci, R. Bruzzese, and S. Amoroso, Laser ablation of silicon induced by a femtosecond optical vortex beam, *Opt. Lett.* **40**, 4611 (2015).
- [31] O. J. Allegre, Y. Jin, W. Perrie, J. Ouyang, E. Fearon, S. P. Edwardson, and G. Dearden, Complete wavefront and polarization control for ultrashort-pulse laser microprocessing, *Opt. Express* **21**, 21198 (2013).
- [32] C. Hnatovsky, V. G. Shvedov, N. Shostka, A. V. Rode, and W. Krolikowski, Polarization-dependent ablation of silicon using tightly focused femtosecond laser vortex pulses, *Opt. Lett.* **37**, 226 (2012).
- [33] J. Wätzel, I. Barth, and J. Berakdar, Ultrafast optically induced resonant and non-resonant current generation in atoms and nanostructures: Role of the photons orbital angular momentum, *J. Mod. Opt.* **64**, 1088 (2017).
- [34] J. Li, H. U. R. Strand, P. Werner, and M. Eckstein, Theory of photoinduced ultrafast switching to a spin-orbital ordered hidden phase, *Nat. Commun.* **9**, 4581 (2018).
- [35] A. S. Moskalenko, Z.-G. Zhu, and J. Berakdar, Charge and spin dynamics driven by ultrashort extreme broadband pulses: A theory perspective, *Phys. Rep.* **672**, 1 (2017).
- [36] M. A. Porras, Effects of orbital angular momentum on few-cycle and sub-cycle pulse shapes: Coupling between the temporal and angular momentum degrees of freedom, *Opt. Lett.* **44**, 2538 (2019).
- [37] Z. Wang, Q. Lin, and Z. Wang, Single-cycle electromagnetic pulses produced by oscillating electric dipoles, *Phys. Rev. E* **67**, 016503 (2003).
- [38] Q. Lin, J. Zheng, and W. Becker, Subcycle Pulsed Focused Vector Beams, *Phys. Rev. Lett.* **97**, 253902 (2006).
- [39] X. Cao, M. Luo, and Z. Wang, Rigorous theoretical model of single-cycle vortex pulse beams produced by oscillating electric dipole arrays, *J. Opt. Soc. Am. B* **37**, 2707 (2020).
- [40] Y. Shen, Y. Hou, N. Papisimakis, and N. I. Zheludev, Super-toroidal light pulses as electromagnetic skyrmions propagating in free space, *Nat. Commun.* **12**, 5891 (2021).

- [41] Y. Shen, A. Zdagkas, N. Papasimakis, and N. I. Zheludev, Measures of space-time nonseparability of electromagnetic pulses, *Phys. Rev. Res.* **3**, 013236 (2021).
- [42] A. Zdagkas, N. Papasimakis, V. Savinov, M. R. Dennis, and N. I. Zheludev, Singularities in the flying electromagnetic doughnuts, *Nanophotonics* **8**, 1379 (2019).
- [43] A. Zdagkas, C. McDonnell, J. Deng, Y. Shen, G. Li, T. Ellenbogen, N. Papasimakis, and N. I. Zheludev, Observation of toroidal pulses of light, *Nat. Photon.* **16**, 523 (2022).
- [44] Y. Fang, M. Han, P. Ge, Z. Guo, X. Yu, Y. Deng, C. Wu, Q. Gong, and Y. Liu, Photoelectronic mapping of the spin-orbit interaction of intense light fields, *Nat. Photon.* **15**, 115 (2021).